4D-Printable Photocrosslinkable Polyurethane-Based Inks for Tissue Scaffold and Actuator Applications

Hossein Goodarzi Hosseinabadi, Arpan Biswas, Anant Bhusal, Ali Yousefinejad, Aastha Lall, Wolfram-Hubertus Zimmermann, Amir K. Miri, and Leonid Ionov*

4D printing recently emerges as an exciting evolution of conventional 3D printing, where a printed construct can quickly transform in response to a specific stimulus to switch between a temporary variable state and an original state. In this work, a photocrosslinkable polyethylene–glycol polyurethane ink is synthesized for light-assisted 4D printing of smart materials. The molecular weight distribution of the ink monomers is tunable by adjusting the copolymerization reaction time. Digital light processing (DLP) technique is used to program a differential swelling response in the printed constructs after humidity variation. Bioactive microparticles are embedded into the ink and the improvement of biocompatibility of the printed constructs is demonstrated for tissue engineering applications. Cell studies reveal above 90% viability in 1 week and ≈50% biodegradability after 4 weeks. Self-folding capillary scaffolds, dynamic grippers, and film actuators are made and activated in a humid environment. The approach offers a versatile platform for the fabrication of complex constructs. The ink can be used in tissue engineering and actuator applications, making the ink a promising avenue for future research.

1. Introduction

Due to its high resolution and high processing rate, digital lighDLP[1,2] has become an attractive industrial additive manufacturing technique. For example, it is adopted for massive production of automotive parts by Desktop Metal and is exploited for large scale fabrication of medical devices, soft actuators, and shoe soles by global corporations such as Medtronic, Boston Scientific, and Adidas, respectively.[3–6] The emerging applications of DLP printing include fabrication of biomedical implants,[7] dental surgical guides,[8] tissue models,[9–11] as well as wax models in jewelry,[12] sculptures in aesthetics,[13] and metamaterials in soft robotics.[14–16] The DLP technique is based on local photocrosslinking of a liquid ink, which mainly consists of monomers/oligomers/macromonomers, a

H. Goodarzi Hosseinabadi, A. Biswas, A. Yousefinejad, A. Lall, L. Ionov
Faculty of Engineering Sciences
Department of Biofabrication
University of Bayreuth
Ludwig Thoma Str. 36A, 95447 Bayreuth, Germany
E-mail: leonid.ionov@uni-bayreuth.de

H. Goodarzi Hosseinabadi, W.-H. Zimmermann
Institute of Pharmacology and Toxicology
University Medical Center Göttingen
Robert-Koch-Str. 40, 37075 Göttingen, Germany

H. Goodarzi Hosseinabadi
Institute for Organic and Biomolecular Chemistry
Department of Chemistry
University of Göttingen
37077 Göttingen, Germany

A. Bhusal, A. K. Miri
Department of Mechanical Engineering
Rowan University
201 Mullica Hill Rd., Glassboro, NJ 08028, USA

W.-H. Zimmermann
German Center for Cardiovascular Research (DZHK)
partner site Göttingen
Germany

W.-H. Zimmermann
Cluster of Excellence "Multiscale Bioimaging: from Molecular Machines to Networks of Excitable Cells" (MBExC)
University of Göttingen
37099 Göttingen, Germany

W.-H. Zimmermann
German Center for Neurodegenerative Diseases (DZNE)
37099 Göttingen, Germany

W.-H. Zimmermann
Fraunhofer Institute for Translational Medicine and Pharmacology (ITMP)
Göttingen, Germany

A. K. Miri
Department of Biomedical Engineering
New Jersey Institute of Technology
323 Dr. Martin Luther King Jr. Blvd., Newark, NJ 07102, USA

A. K. Miri
Department of Mechanical and Industrial Engineering
New Jersey Institute of Technology
323 Dr. Martin Luther King Jr. Blvd, Newark, NJ 07102, USA

**ADVANCED
SCIENCE NEWS**

www.advancedsciencenews.com

NANO · MICRO

small

www.small-journal.com

crosslinker, and a photoinitiator.[9,17] Other components can be added to the ink to modulate its interaction with the light; and thus, affect the resolution of the DLP print. For instance, adding photoabsorbers can adjust light scattering and light absorption kinetics.[2,18] The properties and applications of structures generated by DLP largely depend on the properties of the ink components. Therefore, ink development is one of the main directions in the emerging field of DLP printing.

A highly promising direction in printing is the creation of structures that can evolve and change their properties or shape over time. By considering time as a fourth dimension (4D printing), it becomes possible for the printed structure to change shape when stimulated with moisture,[19] light,[20–22] heat,[14,23] electromagnetic field,[17] and pH.[24,25] 4D printing has strong advantages compared to traditional printing. For example, the conventional DLP-based 3D printing of hollow tubular scaffolds with cells suffers from aggregation and non-uniform attachment of the cells after seeding the cells into the printed tubes,[23] or lack of resolution due to light scattering from the cells membrane.[2,26] In 4D printing, after cell attachment to planar scaffolds, the shape transformation permits the formation of tubular or scroll-like structures with evenly distributed cells on the inner wall of the tubular scaffold.[27–29] A known strategy to build self-folding tubular scaffolds is creating a non-uniformly crosslinked network. By DLP, it is possible to exert control over the light field; and thus, over the photopolymerization reaction, to create non-uniform networks. As the light passes through thickness, some portions of the ink can be fully crosslinked while other portions can be partially crosslinked. The partially crosslinked portion exhibits a higher volume expansion upon swelling which is theoretically,[30] and experimentally,[31] used for fabrication of shape-shifting structures. Recent advances reveal that just by changing the light intensity during DLP printing, it is possible to control the conversion of monomers to form structures ranging from a highly stretchable soft gel to a stiff thermoset polymer.[32]

The biotechnological/tissue engineering applications of the inks used for 4D DLP printing require their proper biocompatibility, which depends on their components. Natural biopolymers, being highly biocompatible, such as gelatin methacrylate (GelMA),[33,34] chitosan methacrylate,[35] carboxymethyl cellulose methacrylate,[36] hyaluronic acid methacrylate (HAMA),[25,37,38] and the silk fibroin produced by a methacrylation process,[39] are commonly used as DLP printing inks. These hydrophilic monomers are naturally derived from biocompatible sources, namely gelatin, chitosan, cellulose, and silk. Their macromonomers usually have large molecular weights ($\overline{M_w} \approx 200\,000$ Da[2,39]), which contribute to a very high viscosity ($\eta \approx M_w^{3.4}$[40]). Therefore, they need to be heavily diluted ($\approx$98% w/v[39]) to reduce the ink viscosity for DLP printing. A drawback of using natural resource-derived monomers is the difficulty in precisely adjusting their molecular weights during purification of the starting material, which may lead to batch-to-batch variability in the final product. Due to their varying molecular weight, they have imprecise biodegradation predictability, which may result in long-term accumulation of the material in vivo and potentially cause unwanted reactions with the host tissue and immune response.[41–43] Developing new synthetic copolymers

allows to improve printing constructs with higher reproducibility and tunability of the biodegradation rate.

Unlike natural-based inks, fully synthetic inks offer the advantage of precise control over the molecular weight of their monomers during the synthesis process. Some synthetic monomers such as bisphenol-A-ethoxylate diacrylate[14] and diurethane dimethacrylate[44] are intrinsically hydrophobic,[29] which makes them improper for transferring nutrients and ingredients in tissue scaffolds and biological environments.[2] Current water-soluble synthetic monomers, such as polyethylene glycol methacrylate (PEGMA) and polyethylene glycol diacrylate (PEGDA) of low molecular weights ($400 < M_w < 600$ Da) result in low viscosities, solvent-free DLP printing, and high resolution constructs.[2] Their printed constructs suffer; however, from brittleness due to high crosslinking density and reaching to the saturation limit in photocrosslinking rapidly, making it hard to achieve a gradient crosslinking as a mechanism for hydrogel 4D printing.[25] Therefore, these individual synthetic inks have rarely found applications in 4D DLP printing.[2] Instead, multi-material printing methods are developed to enable time-dependent shape transformations.[45–49]

A strategy to create new 4D printable inks is mixing different monomers. For instance, mixing PEGDA with tricyclodecanedimethanol diacrylate,[50] or mixing polypentadecalactone diacrylate with polycaprolactone diacrylate,[51] diversifies the molecular mobility. It brings shape memory properties along with high resolution printability for DLP printing of actuators. However, mixing diverse synthetic monomers can compromise the water solubility/biocompatibility of the ink. Overall, synthesis of a new hydrophilic monomer with tunable bimodal molecular weight distribution can expand the range of applications for 4D DLP printing of functional smart materials.

Here, we introduce a new DLP printable ink for creating both tissue scaffolds and actuators. We introduce a method to synthesize a hydrophilic copolymer with customizable bimodal molecular weight distribution. With our synthetic monomer, we unlock the ability to fine-tune the molecular weight without compromising water solubility, printability, and resolution. This can help to adjust the molecular weight to reveal both controlled biodegradation rate and high-resolution printability. Further, our ink demonstrates exceptional biocompatibility, making it ideal for biomedical applications. The versatility of the ink is shown by creating self-folding scaffolds, grippers, and actuators, to highlight its broad range of applications. We embed bioactive glass particles into the ink to enhance the biocompatibility of the printed smart material.

2. Results and Discussion

The concept of 4D shape transformation of a DLP printed film is illustrated in **Figure 1**a. We use a water-based solution of a photocrosslinkable monomer as the ink, which is selectively illuminated with blue light (405 nm) in a layer-by-layer manner, following the standard procedure of DLP 3D printing. By adjusting the exposure time and light intensity during DLP printing, we aim to create a vertical gradient of crosslinking density within the crosslinked gel. After the DLP printing process, the crosslinked gel is dried (Figure 1a-ii) and then immersed in water,
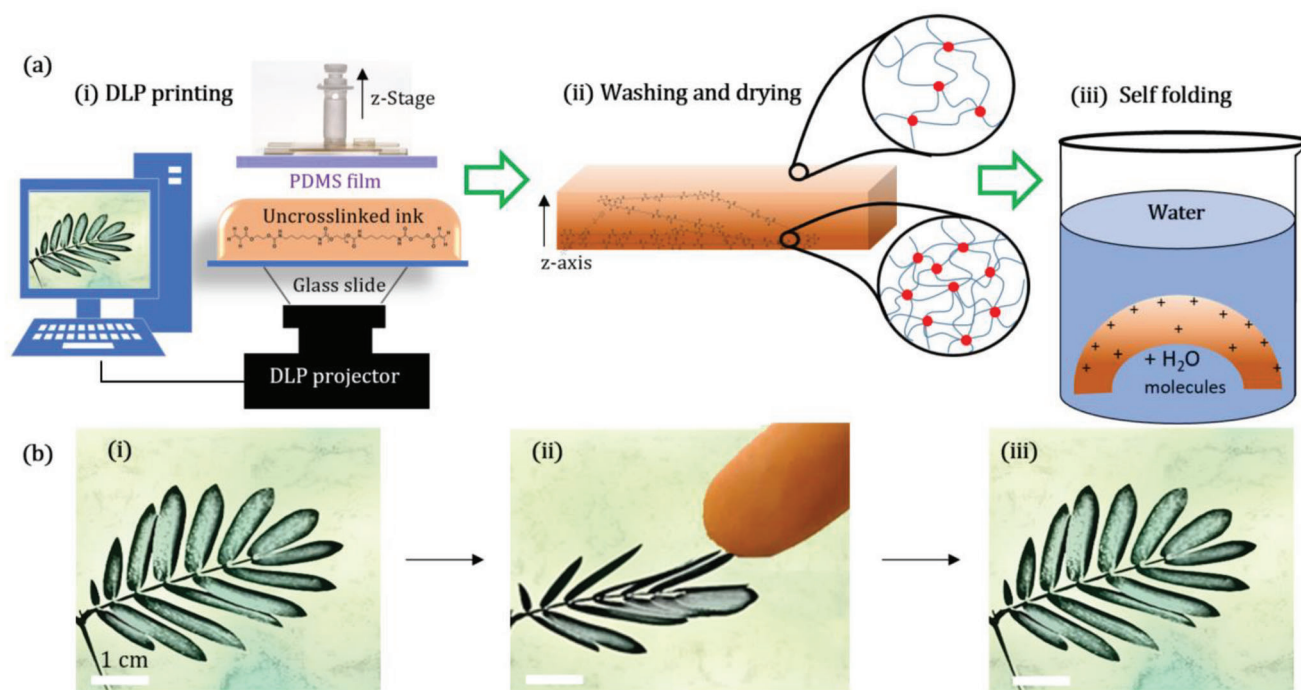
Figure 1. Scheme of 4D DLP printing: a) introducing the concept of 4D shape transformation by: a-i) programmable DLP printing of the ink, a-ii) washing and drying of the film with vertical gradient crosslinking, and a-iii) immersing the film into water to initiate self-folding behavior; when the hydrogel film is exposed to water, the upper layer having fewer crosslinking sites absorbs more volume of water molecules compared to the lower layer; and consequently, the construct starts to self-fold in the new environment. b) Analogy to reversible self-folding behavior in *Mimosa pudica* plant in nature: b-i) initial state, b-ii) shape transformation upon exposure to the stimulus, and b-iii) shape recovery after elimination of the stimulus (inset: 1 cm).

resulting in inhomogeneous swelling (Figure 1a-iii). This inhomogeneous swelling induces bending of the printed and dried object, enabling the creation of various 3D shapes. Upon drying, the gel reverts to its initial 2D/flat structure. The idea of our approach is inspired by shape transformation observed in plants. Motion in plants is a highly nontrivial process which is often based on anisotropic swelling driven by variation of water content within the leaf tissue.[52] Figure 1b shows an analogy to an apparently similar behavior in the leaves of the Mimosa–pudica plant. Upon exposure to an external stimulus such as finger proximity, water is removed from the leaf base. The mechanism forms a gradient distribution of water, leading to leaf folding in response, making them flaccid (Figure 1b-ii). Once the stimulus is removed, the leaf gradually restores its initial water distribution, eliminating the gradient and returning the fresh leaves to their original shape (Figure 1b-iii).

In order to enable shape transformation of the printed structure through swelling, we developed a special ink (**Figure 2**a), which is based on a water-swellable photocrosslinkable copolymer. PEG-aliphatic polyurethane (PEG-PU) copolymers were synthesized using a two-step polymerization technique. The first step involved the growth of polymer chains through a reaction between polyethylene glycol diol and hexamethylene diisocyanate. In the second step, acrylate groups were introduced at both ends of the polymer chain, resulting in polyethylene glycol–polyurethane diacrylate copolymer (PEG-PU-DA). The polymerization time should allow for control over the molecular weight of PEG-PU-DA chains, which could be utilized to tune the mesh size of the polymer network obtained through photocrosslinking in the 3D printing process.

The composition of the synthesized PEG-PU-DA copolymer was assessed using ^{1}H-NMR spectroscopy,[53,54] (Figure S1a, Supporting Information). The presence of acrylate hydrogens in our synthesized ink was confirmed by signals observed at 5.80, 6.07, and 6.38 ppm. These acrylate anchors make the copolymer suitable for DLP printing. The signal observed at 7.20 ppm corresponds to the hydrogens of the N—H group in the urethane linkage. The signals demonstrate the successful formation of functional groups during the synthesis process illustrated in Figure 2a.

The copolymers obtained at different polymerization times (Rt: 15, 45, and 60 min) exhibited a multimodal molecular weight distribution (Table S1, Supporting Information; Figure 2b). Gel permeation chromatography (GPC) measurements were calibrated using a refractive index (RI) detector and polystyrene (PS) as a standard, providing relative values of molecular weight rather than absolute values. One peak was observed at ≈7 kDa, which could be attributed to a mixture of PEG-diol (Mw = 3000 g mol^{-1} according to information from Sigma–Aldrich; $M ≈ 5000$ g mol^{-1} according to our measurements) and PEG-diol reacted with one or two diisocyanate molecules. The largest peak appeared at ≈40–50 kDa, and the positions of these two peaks were relatively unaffected by the reaction time. However, increasing the reaction time led to the emergence of a shoulder at very high molecular weight (>100 kDa) and a decrease in the amplitude of the peak at 40–50 kDa, while the amplitude of the peak at 7 kDa remained
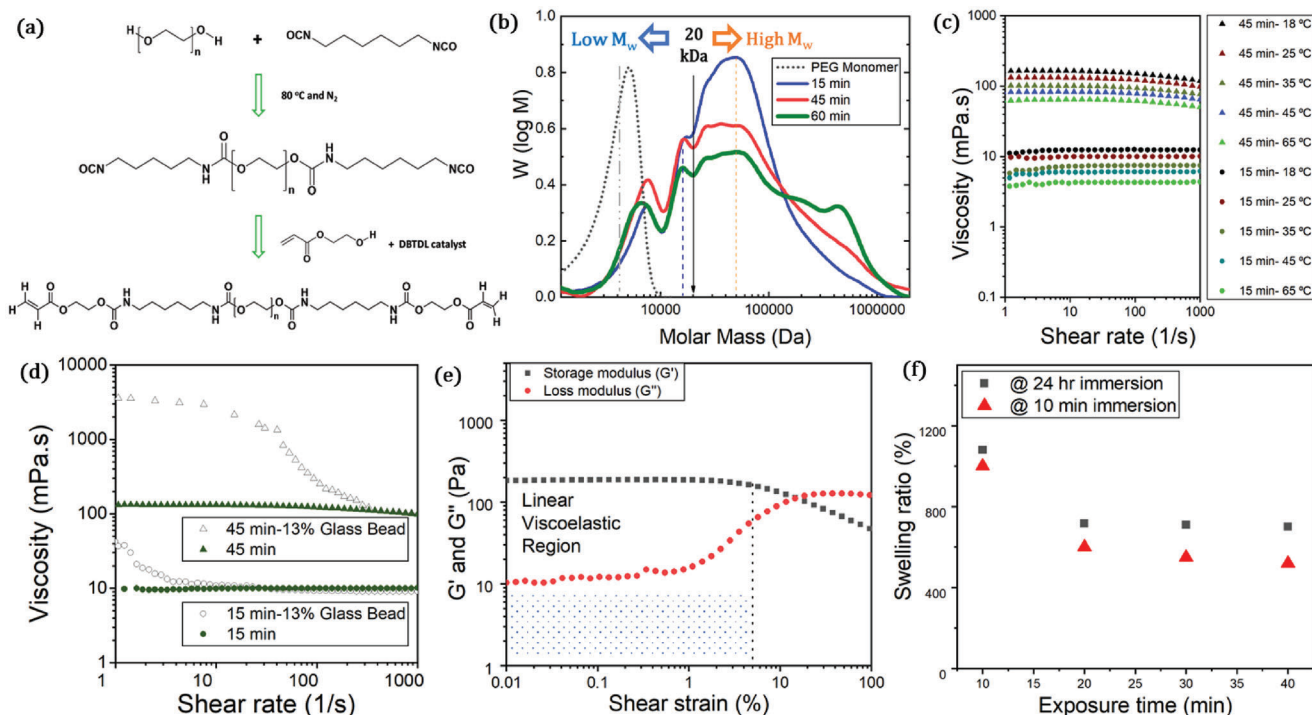
Figure 2. Properties of DLP inks: a) two-step polymerization used for synthesis and the molecular structure of the synthesized ink; b) GPC data showing possibility of adjusting the ink multi-modal molecular weight distribution with varying the reaction time; c) rheological properties of the inks show increasing zero-shear viscosity with increasing the reaction time and decreasing the ink temperature; d) rheological properties of the inks synthesized by 15 and 45 min reaction times show that adding glass increases zero-shear viscosity of the ink; e) amplitude sweep tests show hydrogel network formation with a limit of 5% shear strain to remain in the linear viscoelastic region ($\tau = 9$); f) swelling ratio is continuously decreased by increasing the light exposure time, after 10 min immersion; however, swelling ratio reaches to a saturation state after 24 h immersion (all samples crosslinked with 2 mW cm^{-2} light intensity at 400 nm wavelength).

nearly unchanged. Thus, the copolymer mixture consisted of PEG-diol and diisocyanate-modified PEG-diol along with a high-molecular-weight polymer whose molecular weight could be controlled by varying the polymerization time. The modification with acrylate groups was anticipated to have minimal impact on the molecular weight of the polymer.

As expected, an increase in molecular weight (by increasing R_t) led to higher melting temperatures (T_m: 46.6 °C, 47.1 °C, and 47.6 °C for R_t: 15, 40, and 60 min, respectively), crystallization temperatures (T_s: 25 °C, 29 °C, and 35 °C for R_t: 15, 40, and 60 min, respectively), and crystallization enthalpy (Figure S1b, Supporting Information). It is noteworthy that although HDI links PEG chains together and increases molecular weight (resulting in a weaker contribution of chain ends to entropy), the melting temperature of the polymer is considerably lower than that of the pure PEG monomer used in this work ($T_m = 60$ °C). This discrepancy could be attributed to imperfections and hindered rotation around chemical bonds caused by urethane groups.

We then investigated the rheological properties of water solutions of the synthesized polymers with different molecular weights as 3D printing inks (Figure 2c). For the inks synthesized at a 15 min reaction time, the viscosity-shear rate response of the ink solution (15 wt% polymer) exhibited near Newtonian fluid behavior within the measured shear rates (1–1000 s^{-1}). As the reaction time increased to 45 min, the ink solution showed an eightfold increase in viscosity and notable shear thinning behavior at

shear rates above 10 s^{-1}. Shear thinning was a landmark of disentanglement in polymer chains during flow, occurring when the shear rate exceeded the reciprocal relaxation time (0.1 s), indicating a higher molecular weight at a reaction time of 45 min compared to 15 min. The viscosity of the ink moderately decreased with increasing temperature (see plot of zero shear viscosity, η, versus $1/T$ in Figure S1c, Supporting Information), and the activation energy remained nearly independent of molecular weight ($E_{A(Rt: 15\ min)} = 18.5$ kJ mol^{-1}, $E_{A(Rt:\ 45\ min)} = 19.8$ kJ mol^{-1}; Figure S1c, Supporting Information). The viscosity of the polymer solutions used as inks, at the selected concentration, remained well below the upper limit for stereolithography 3D printing (i.e., 10^4 mPa · s$^{[55,56]}$). Bioactive glass particles with an average diameter of 4 µm were added to the polymer solution, which is an approach for simulating the light scattering influenced by cells during DLP bioprinting.[2] The particles maintained a homogenous distribution during DLP printing over a time scale of 30 min, attributed to slow sedimentation due to adequately high viscosity of the polymer solution. The addition of bioactive glass particles (13 wt%) led to a considerable change in the rheological behavior of the polymer solution. The viscosity at low shear rates considerably increased, possibly due to interactions between particles. High shear rate resulted in shear thinning due to break of contacts. The values of the viscosity at both low and high shear rates remained below the limit required for stereolithography (Figure 2d).

ADVANCED
SCIENCE NEWS
www.advancedsciencenews.com

NANO · MICRO
small
www.small-journal.com

Next, we studied the mechanical properties of crosslinked and dried polymer films. To prepare the samples, the inks obtained at different reaction times were mixed with 3:30 mM Ru:SPS photoinitiator[57,58] and exposed to the low intensity light (2 mW cm^{-2}) by SLA 3D printer for various exposure times to create rectangular films for tensile testing. The stress–strain response (Figure S1d, Supporting Information) of the dried films (oven-dried at 60 °C overnight) revealed that increasing the exposure time led to an increase in the elastic modulus of the films (E = 126, 146, and 190 MPa for $t_{exposure}$: 15, 30, and 45 min, respectively). The elastic modulus exhibited a proportional increase with longer light exposure times due to the higher crosslink density. Increasing the reaction time resulted in higher elongation at break and toughness, while decreasing the elastic modulus (ϵ_{break} = 5% and 14%, U_T = 31 and 71 J m^3, E = 190 and 56 MPa for R_t = 15 and 45 min, respectively). This behavior is commonly observed, as an increase in molecular mass leads to greater elongation at the break due to the increased degree of curtailment of polymer coils ($\langle R_n^2 \rangle = n \times l^2$, where R is average end-to-end distance, and n and l are number and length of segments, respectively). The elastic modulus decreases with increasing molecular weight of the ink because a higher molecular weight results in a lower number of acrylate terminal groups, which likely leads to a lower crosslinking density after photocrosslinking; and consequently, a lower elastic modulus.

Mechanical spectroscopies comprised of an amplitude sweep and a dynamic frequency sweep were performed to characterize the polymer network swollen in MilliQ water with a swelling degree of ≈600%. In the amplitude sweep, the hydrogel was subjected to 0.01–100% shear strain sweeps at a constant frequency of 1 rad s^{-1} (Figure 2e). Within the range of up to 5% shear strain, a linear viscoelastic region was observed where the storage modulus, G', remained independent of the applied shear strain (Figure 2e), and G' dominated the loss modulus, G''. Frequency sweep experiments at a constant shear strain (0.5%) also revealed a linear viscoelastic region across the frequency range, with G' dominating G'' and both G' and G'' being independent of the applied frequency (Figure S1e, Supporting Information). These results confirm the formation of an elastic gel network.

The swelling response of the photocrosslinked hydrogels varied depending on the exposure time. Increasing the exposure time resulted in a decrease in the swelling ratio (Figure 2f). This can be attributed to the expected increase in crosslink density with longer exposure, leading to reduced water uptake. The swelling response of the hydrogels was also observed to be time-dependent (compare swelling ratios at 10 min and 24 h after immersion). The dynamic of the swelling response could be effectively controlled by adjusting the exposure times, allowing for precise manipulation of the hydrogel behavior.

To create tailored geometries with the ink (R_t = 15 min) under low and high light intensities, we utilized two different setups: I) we used a stereolithography (SLA) printer which allowed printing at a very low intensity light (i.e., 2 mW cm^{-2} at 400 nm wavelength) and increased photocrosslinking time (≈10 min exposure); as the experiments were time consuming and the optimal printing parameters were not trivial; here, we needed to calibrate several parameters using a design of experiments (DOE) methodology as will be discussed in the following paragraph; II) we separately used a custom-built DLP printer which allowed ink printing at a very high intensity light (700 mW cm^{-2} at 380 nm wavelength). The exposure time at this high intensity was decreased down to 400 ms, allowing to print in very short times and to quickly calibrate the setup. Here, we didn't need to conduct another DOE for calibration of the printing parameters. Instead, we optimized the printing exposure time based on the observed folding behavior as will be discussed under Figure S2, Supporting Information.

The stereolithography printer operating at a low light intensity (2 mW cm^{-2} at 400 nm wavelength) was used to study the impact of exposure time, dye, and glass content on the quality of printed structures (particularly in terms of cure depth and printing resolution, given that cure area ratio = 1 represents the optimal printing resolution). The ink was prepared by homogenously mixing different concentrations of the bioactive glass material (i.e., 45S5[59]). The material was known for having a refractive index close to that of cell membranes ($n \approx 1.34$); therefore, the glass could simulate the light scattering effects relevant to tissue engineering applications.[26] In addition, a food dye (Ponceau 4R) was used as a photo absorber to enhance printing resolution by minimizing potential light scattering effects.[57] The ink solution was subjected to a triangular light pattern, achieved by uploading a triangular digital photomask onto the printer. To optimize the printing conditions, a design of experiment (DOE) methodology was employed, specifically utilizing a fractional factorial method with a center point. This approach allowed for the reduction in the number of experiments conducted, and a total of nine experiments were carried out to determine the optimal printing conditions for the triplet variables (**Figure 3**a).[60]

The conducted experiments provided a basis for statistical evaluation using MiniTab software (2D plots revealing the variation of both cure depth and cure area are illustrated in Figure S1f, Supporting Information). As complementary graphs for better visualization of a part of the 2D plots, the statistical variations of the cure depth versus exposure time, glass content, and dye content were calculated by MiniTab and illustrated in 3D plots in Figure S1g,h, Supporting Information. The 2D plots led to the following conclusions. Increasing the exposure time resulted in improved cure depth and cure area ratio (cure area ratio = gel area/photomask area), which was potentially attributed to increased penetration depth and light scattering effects (Figure S1f, Supporting Information). Conversely, increasing the dye content led to a decrease in both cure depth and cure area ratio, likely due to enhanced light energy absorption by the dye. The addition of glass microparticles reduced light penetration by causing reflection and scattering of incident light on the glass surface; thus, reducing the cure depth. The glass particles were observed to reflect and scatter light, redistributing it in non-illuminated areas instead of allowing it to penetrate deeper. As the light reflection from the glass surfaces increased, the cure area ratio also increased proportionally with the glass content (Figure S1f, Supporting Information). Statistical optimization using MiniTab revealed that incorporating 13% glass microparticles could maximize the algebraic summation of the cure depth and the printing resolution (the difference between the printed gel area and the photomask area).[60] Triangular patterns were printed with and without 13% glass microparticles, and their enlarged surface micrographs illustrated in Figure 3b. Morphological analysis of the swollen hydrogels showed that the incorporation of glass
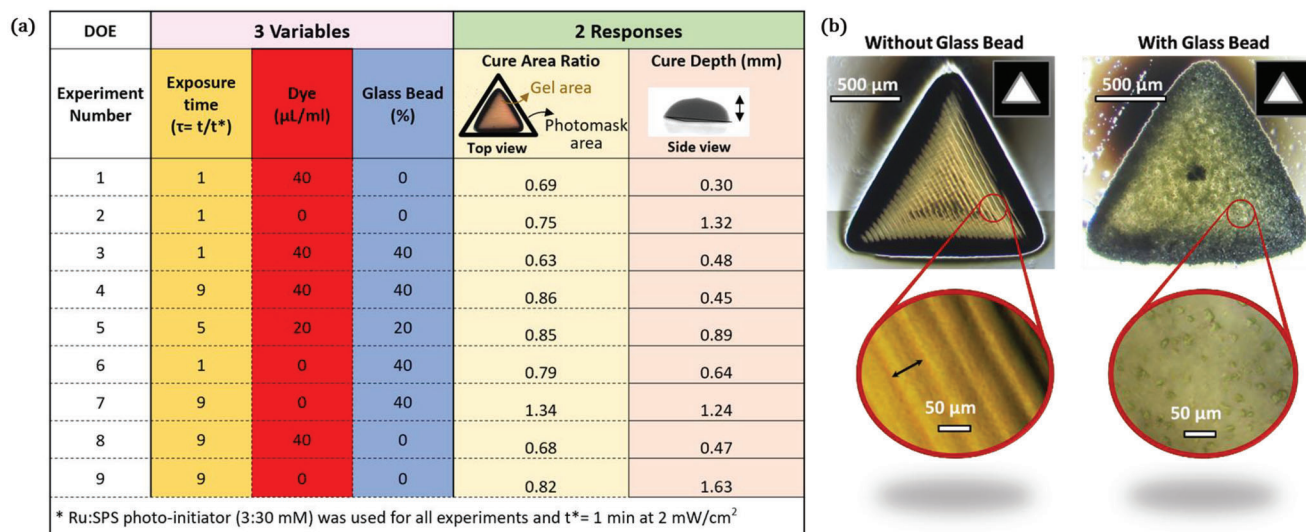
DOE	3 Variables			2 Responses	
Experiment Number	Exposure time (τ= t/t*)	Dye (μL/ml)	Glass Bead (%)	Cure Area Ratio (Top view)	Cure Depth (mm) (Side view)
1	1	40	0	0.69	0.30
2	1	0	0	0.75	1.32
3	1	40	40	0.63	0.48
4	9	40	40	0.86	0.45
5	5	20	20	0.85	0.89
6	1	0	40	0.79	0.64
7	9	0	40	1.34	1.24
8	9	40	0	0.68	0.47
9	9	0	0	0.82	1.63

* Ru:SPS photo-initiator (3:30 mM) was used for all experiments and t*= 1 min at 2 mW/cm^2

Figure 3. Role of adding bioactive microparticles to the ink: a) the design of experiments for three variable factors changing at three levels and the measured values for two responses obtained after image analysis; b) optical micrographs of printed hydrogels at the optimized printing conditions show formation of a more homogenous surface morphology with using the glass microparticles possibly due to increased light scattering from glass surface (samples printed with 2 mW cm^{-2} intensity at 400 nm wavelength).

particles in the ink made the crosslinking associated with light reflections from the sharp edges of the photomask pixels less visible. We observed that the light scattering effect of glass microparticles increased the homogeneity of photocrosslinked structure by compromising the reflections from the pixel edges. It was also observed that the addition of this amount of glass particles to the ink did not significantly alter the elastic modulus and elongation at break of the printed films (Figure S1–i, Supporting Information). Therefore, it can be assumed that incorporating 13% glass particles in the ink formulation would not significantly impact the mechanical response of the printed hydrogels.

We investigated the time-dependent shape transformation of crosslinked films. We found that upon immersion into water, the film first folded quickly and strongly (see Movie S1, Supporting Information); and then, it preserved its tubular shape for a long period of time (observed up to 6 months) before the material degraded. We believe that the folding phenomenon takes place due to differential swelling of PEG segments at the molecular scale. Apparently, each flat film consists of sections having different crosslinking densities; thus, having different kinetics of swelling: an upper section that swells quickly and notably, inducing immediate rolling, and a lower section that swells more slowly, contributing to gradual swelling. According to the literature in similar self-folding hydrogel systems having gradient crosslinking through thickness,[25] the diameter of the resulting tube is dependent on the film's thickness. The film thickness can be correlated to the duration of light exposure during the printing process (for instance the correlation is measured for SLA printer in Figure S1–j, Supporting Information) or can be adjusted with setting the z stage distance (as shown in the DLP printer setup in Figure 1a). Remarkably, the tube radius remains almost unchanged after 10 min and 24 h of immersion in water (Figure S2, Supporting Information).

We demonstrated the fabrication of solid and porous tubular scaffolds with pH responsive properties. These scaffolds hold great promise for various tissue regeneration applications as they can replicate the internal diameter of the vessels, venules, and capillaries in human organs,[24] as well as serve as artificial nerve grafts for neuron regeneration.[27] The ink solution (synthesized at R_t: 15 min) was mixed with LAP (0.03% w/v) and exposed to a rectangular photomask (1.5 × 1 mm^2) using a high intensity DLP printer (≈700 mW cm^{-2}). After washing and drying the resulting flat rectangular hydrogels, they were immersed in water, leading to a remarkable self-folding response (**Figure 4**a). Using our approach, we were able to create high resolution and robust tubular scaffolds with diameters as low as 190 ± 10 μm diameter ($t_{exposure}$ = 0.4 s, Figure 4a). We found that very short exposure times (<0.3 s) were insufficient for creating robust/sturdy structures while very long exposures (>2.5 s) led to the formation of semi-folded tubes with larger radius (Figure S2, Supporting Information). Intermediate times in the range 0.4 s < $t_{exposure}$ < 1 s were optimal to allow creation of robust and small tubular scaffolds. We hypothesized that long exposure times result in more saturated crosslinking across the film cross sections, reducing the gradient of crosslinking through thickness that is crucial for self-folding. Therefore, longer exposures lead to weaker folding, which aligns our observations with the hypothesis. Further, we extended our technique to produce films with specific porosity patterns (e.g., 12 square holes of 200 μm length distributed over a 1.5 × 1 mm^2; Figure S3c, Supporting Information). These films were DLP printed, washed, dried, and immersed in PBS to induce self-folding and form porous tubular scaffolds. Interestingly, both the tube diameter and the size of the porosities exhibited pH-responsive behavior (Figure 4b). The changes in ion concentration associated with pH variations may cause modifications in the intermolecular forces of the hydrogel network, thereby affecting the porosity and tube dimensions.

To demonstrate the scalability of our technique, we printed a larger porous pattern composed of 90 porosities over a 3 × 4 mm^2 surface in only 400 ms of light exposure. Upon immersion in the

ADVANCED
SCIENCE NEWS

www.advancedsciencenews.com
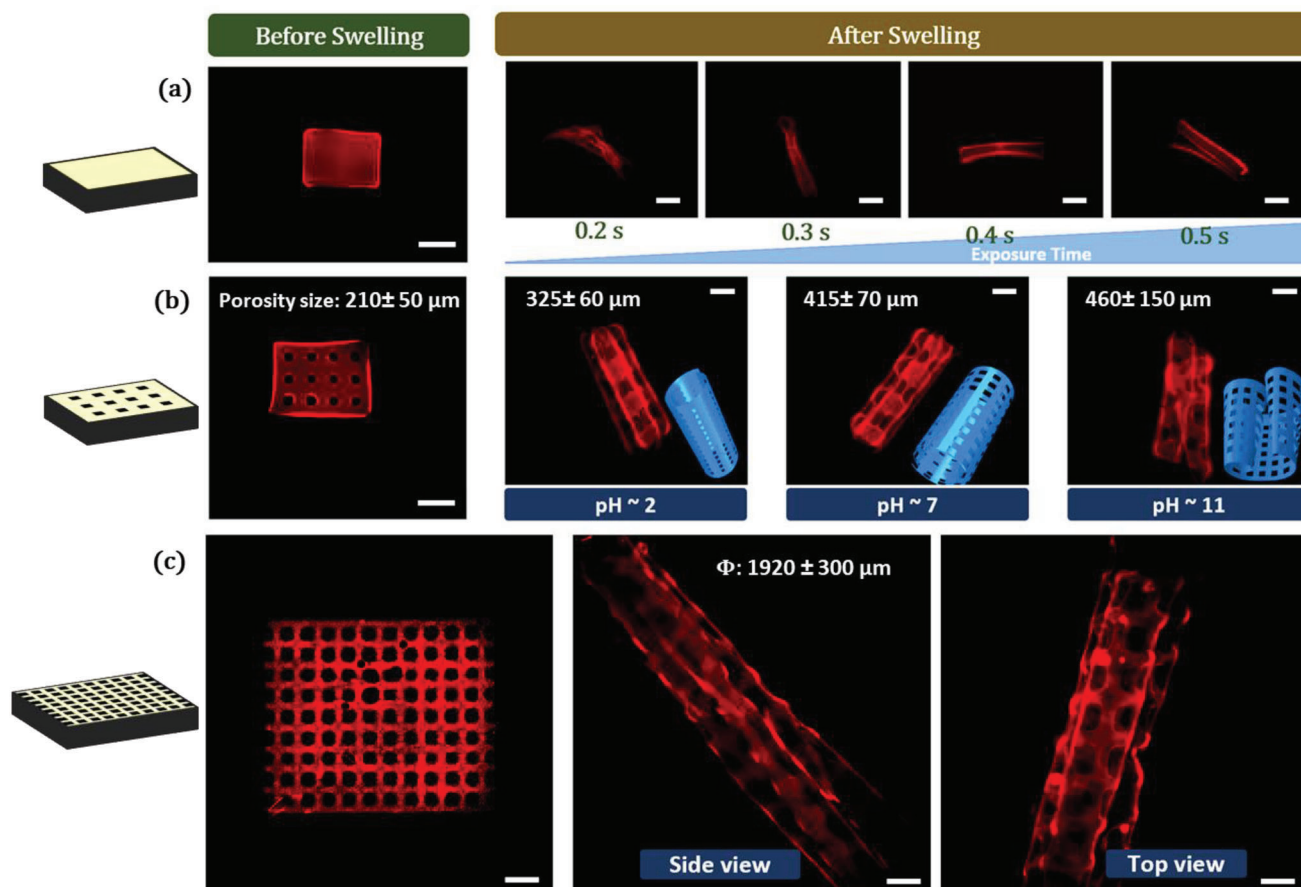
NANO · MICRO
small
www.small-journal.com

Figure 4. Tubular scaffold fabrication using PEG-PU-DA for tissue regeneration. a) Tubular scaffolds fabricated by immersing the printed patterns at different exposure times using the high intensity DLP printer (inset 900 µm). b) Programmable porous tubular scaffolds formed by immersing the pattern composed of 12 square holes of 200 µm length distributed on a 1.5×1 mm^2 area and the pH sensitivity of their geometries. c) Fabrication of a more complex porous tubular scaffold using a photomask composed of 90 square porosities distributed over a 3×4 mm^2 surface (samples crosslinked with 700 mW cm^{-2} intensity at 380 nm wavelength, 400 ms).

culture media, a tubular porous scaffold of $\approx 1.9 \pm 0.3$ mm diameter was created (Figure 4c). Such a biocompatible porous tubular scaffold architecture would have been challenging, time consuming, and might be clinically impossible to produce using conventional fabrication techniques such as two-photo polymerization or electrospinning and further machining processes.[61–63]

To explore the biomedical applicability of our printed scaffolds, we conducted several assays on biodegradability, cell attachment, and cell proliferation (**Figure 5**a). The scaffolds exhibited a degradability of up to 50% after 4 weeks of immersion in water which is close to that of other PEG-based hydrogels reported in the literature, such as four-arm-PEG.[64] This level of degradability suggests that our scaffolds have the potential to degrade over time in biological environments.

The biocompatibility of scaffolds was investigated by culturing MC3T3-E1 cells on the DLP printed scaffolds, both with and without the presence of bioactive glass microparticles, for a period of 7 days. A live/dead assay was performed, revealing around 90% cell viability (Figure 5b,c). In addition, an alamarBlue assay was conducted, indicating an increasing cellular activity over the 7-day incubation period (Figure 5d). These results demonstrate the compatibility of the PEG-PU-DA scaffolds with cell attach-

ment and proliferation, indicating their potential use in tissue engineering. The strong biodegradability and cellular compatibility of the scaffolds further support their suitability for a wide range of biomedical applications.

Finally, we explored the actuator and sensor applications of the DLP printed constructs. For the actuator demonstration, a simple rectangular structure was produced by printing two layers, each having ≈ 100 µm thickness using low intensity light (2 mW cm^{-2}, **Figure 6**a). A gripper structure composed of four rectangular blades was created by printing another set of two-layers, each having ≈ 100 µm thickness using high-intensity light (700 mW cm^{-2}, Figure 6b). In both cases, the 2nd layer was printed with a ten-fold higher exposure time compared to the 1st layer, and the thickness of each layer was set to ≈ 100 µm by adjusting the z-stage. After the DLP printed patterns were gently washed, dried, and immersed into water, we observed a transient shape transformation in both structures. The transformation started with folding (toward the 2nd layer) and subsequent unfolding of the structure (Figure 6a,b). This sequential folding–unfolding is likely a result of different kinetics of swelling between the 1st (less crosslinked) and 2nd (more crosslinked) layers, caused by variations in their different crosslinking densities. The different crosslinking times
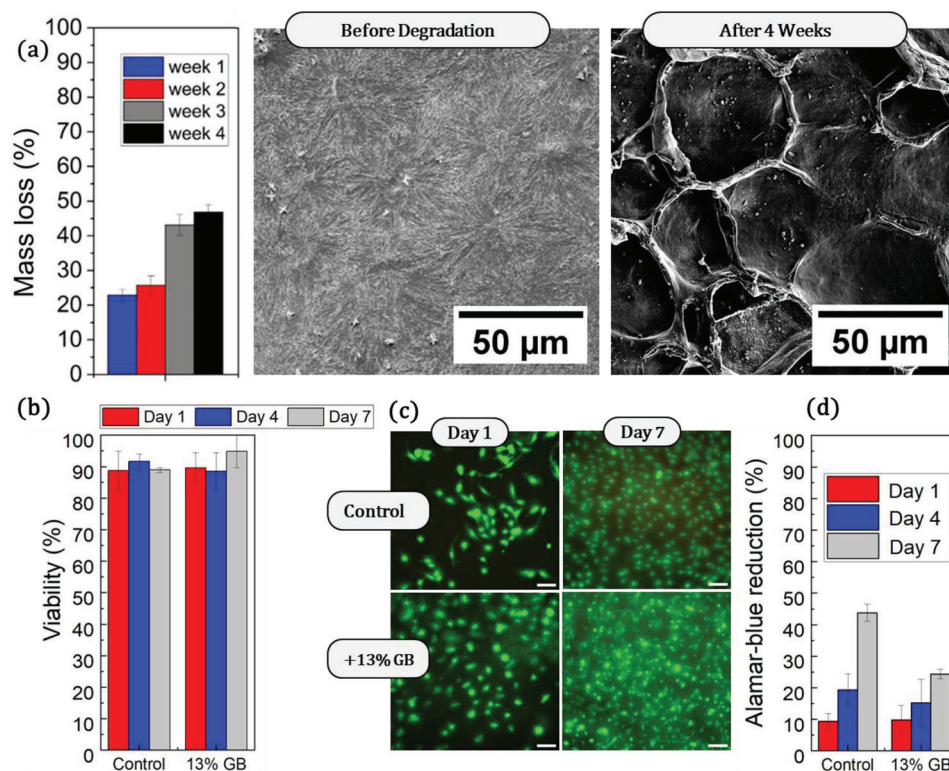
Figure 5. Biocompatibility and biodegradability studies. a) Degradation tests revealed up to 50% mass loss after 4 weeks of immersion in PBS. b) Live–dead assay results showing above 90% viability after 7 days of culturing MC3T3-E1 cells on DLP printed films without (control) and with 13 wt% glass beads. c) Images obtained from the cell studies after 1 day and 7 days (inset: 100 µm). d) alamarBlue assay demonstrating an increased cellular activity/metabolism with and w/o bioactive glass after 1, 4, and 7 days of culture on PEG-PU-DA films. All samples prepared with 3:30 mM Ru:SPS photoinitiator under 2 mW cm^{-2} intensity at 400 nm wavelength, $\tau = 9$.

applied during printing lead to distinct crosslink densities, diffusion rates, and relaxation times between the 1st and 2nd layers. The time lapse images in Figure 6a,b illustrate the folding and unfolding processes over time. The closure and opening of these two structures occurred on different timescales, with a duration of 600 s under low light intensity (Figure 6a) and 90 s under high light intensity (Figure 6b). This demonstrates the versatility of the ink formulation as it allows the creation of actuators that can respond to external stimuli on a programmable timescale by utilizing different light parameters. The DLP device capability to precisely control the design parameters such as the light intensity, exposure time, and the layers thickness enables the fabrication of structures that exhibit programmable shape transformations in response to humidity stimuli, opening up possibilities for various dynamic applications.

The capability of the material to act as a mechanical gripper was evaluated by attaching a simple one-layer rectangular film (6 mm × 18 mm × 100 µm prepared at 2 mW cm^{-2}) to a transparent glass straw and pumping humid air to perform some tasks such as grasping, lifting, transporting, and releasing a foam object in response to controlled changes in humidity (see Movie S2, Supporting Information). The gripper could load an object (≈50 mg, five times the film weight) and carried it under continuous pumping of humid air (RH ∼ 90%, 10 mL s^{-1} flow rate). As soon as pumping humid air was stopped, the film started to dry out, unload the object, and return to the unfold state.

We also investigated the sensitivity of our printed films to atmospheric moisture. In this experiment, a dried printed film was installed in a free-standing form on a glass Petri dish (Figure 6c). We observed that when a finger was pointed toward the film without physical contact at ≈1 cm distance, the film would fold to escape from the humid skin surface. Water molecules present in the surrounding atmosphere were in equilibrium with the surfaces of the PEG-PU-DA film. The surface closer to the finger adsorbed more water molecules, creating a higher humidity level, while the opposite surface of the film equilibrated with the less humid atmosphere. This unbalanced distribution of water molecules on the two sides of the film likely resulted in a gradient of H$_2$O distribution through the film thickness. Like a cantilever beam, the film rapidly initiated folding in less than 1s. Once the finger was removed, the humidity levels on both sides of the film returned to equilibrium with the same atmosphere (Figure 6d). Consequently, the film reversibly returned to its original standing shape, allowing for apparently unlimited consecutive folding and unfolding cycles. In a prior publication, a comparable folding behavior in response to skin humidity was documented within a cellulose nanofiber-based composite film.[65] The authors proposed that the strong hydrogen-bonding interactions in this polymer form a continuous and highly efficient 3D network structure for effective transport of water molecules in response to minor variations of the atmospheric humidity. As in our polyurethane system, isocyanate (NCO) groups exist which are known for
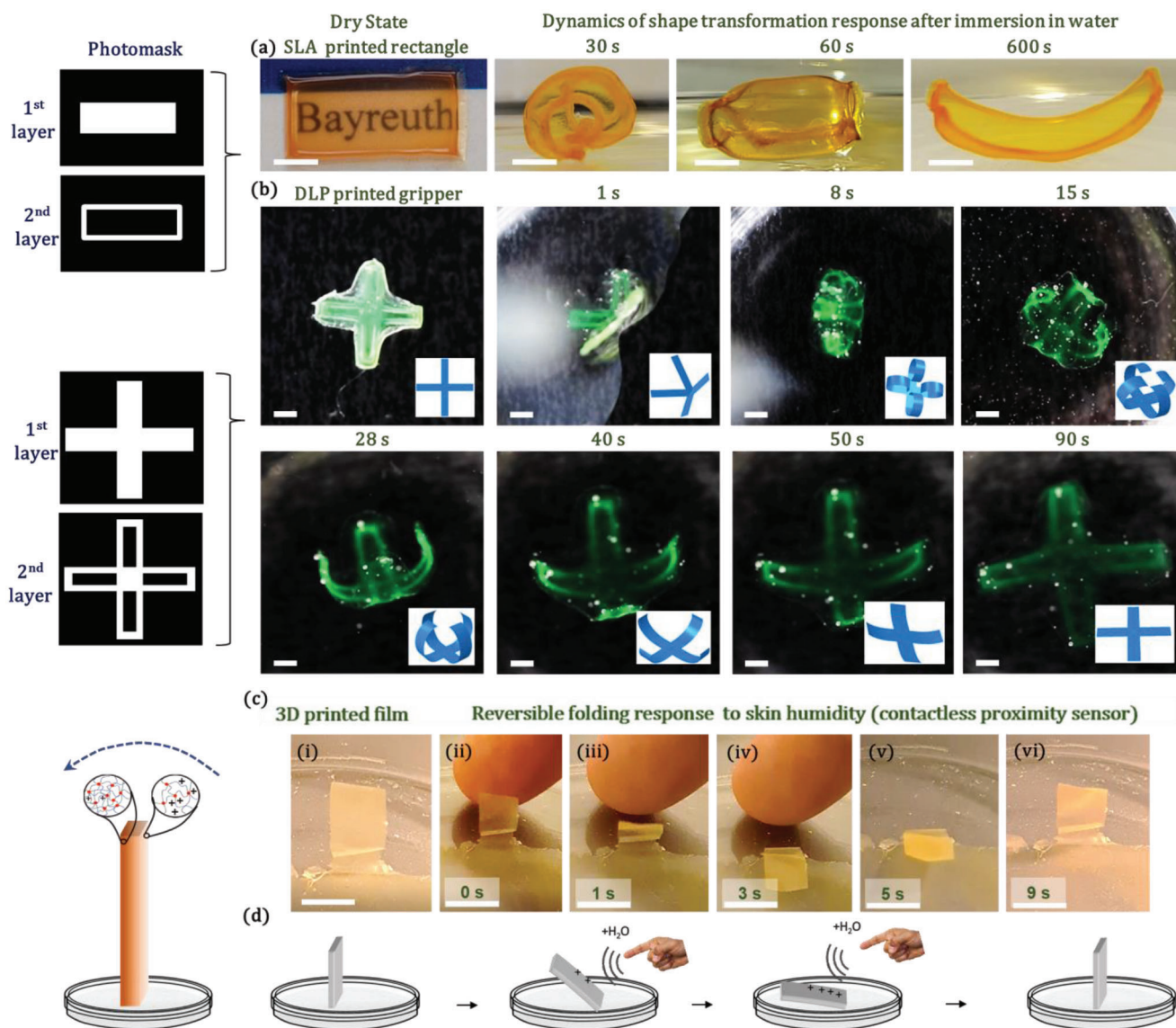
Figure 6. Actuator application. a) A rectangular structure is printed with two layers using the low intensity light (2 mW cm^{-2} intensity at 400 nm, scale bar: 1 mm). b) A gripper structure is printed with two layers using the high intensity light (700 mW cm^{-2} intensity at 380 nm wavelength, 400 ms, scale bar: 1 mm). The structures were dried and immersed in water. Dynamic self-folding and unfolding of the structures are shown in the time-lapse. c) PEG-PU-DA film is printed (2 mW cm^{-2} intensity at 400 nm, $\tau = 9$) and installed on a glass Petri in standing form; finger was placed nearby the standing film without physical contact (distance $\approx$ 1 cm) and was removed after seconds; the film reversibly showed folding/unfolding response (scale bar: 1 cm). d) Schematic representation of the film behavior with regard to absorption/desorption of water molecules (+) from the surrounding atmosphere.

formation of robust hydrogen bonds, it can be reasonable that a similar mechanism contributes to the observed folding behavior in our printed films in response to variations of the atmospheric humidity.

The dynamics of the folding behavior was dependent on the film thickness. A film having 50 μm thickness folded over five times faster compared to a film of ≈150 μm thickness (Movie S3, Supporting Information). The reversible shape transformation was bi-directional as demonstrated in the Movie S4, Supporting Information. In addition, we extended our investigation by exposing the film to an open flame for evaluating the influence of heating at higher temperatures. Folding was not observed until

the film edge was partially melted (Movie S5, Supporting Information).

We repeated the folding experiment by exposing a circular printed film, 150 μm thickness, to a human hand's palm, characterized by elevated moisture and heat due to its larger surface area compared to finger. We utilized thin gloves that could block humidity transfer but were transparent to the body heat (33 °C at the surface). We observed that the folding did not occur due to the palm heat. Instead, moisture was the exclusive trigger for the folding. The response of the film actuator was bi-directional, meaning that by rotating the film, the folding direction was fully reversed (see Movie S6, Supporting Information).

The folding behavior of the film may remind us of the behavior of leaves of *Mimosa-Pudica*, which exhibit self-folding and unfolding responses when subjected to an external stimulus (Figure 1b). Both *Mimosa* leaves and the printed films here are escaping from an external stimulus. While the folding behavior of Mimosa leaves has evolved over ≈90 million years through a complex mechanism,[66,67] here, we introduced a fully synthetic material that replicated shape transformation, apparently comparable to a folding leaf. In the past, mostly non-synthetic (i.e., natural) materials such as *Bacillus subtilis* spores[68] and cellulose fibrils[69] were utilized to build humidity actuators that could fold like leaves. To this aim, synthetic components were mostly utilized in the form of a mixture with natural components that could intrinsically contribute to the transport of water molecules. For instance, multi-material composite structures obtained from mixing graphene oxide, carbon nanotube, and cellulose were able to show self-folding due to skin proximity.[65] In our case, a single synthetic ink was developed for light assisted printing of self-foldable architectures upon exposure to atmospheric humidity variations.

By harnessing the moisture responsiveness of the light assisted printed films, we have achieved a biomimetic behavior reminiscent of natural systems. This finding highlights the potential of our synthetic material for various applications, including adaptive structures, responsive sensors, and soft robotics, where reversible shape changes in response to environmental stimuli are desired.

3. Conclusion

In this study, we synthesized hydrophilic poly (ethylene-glycol)-based polyurethane copolymers and formulated an ink for light assisted printing. The printed synthetic material enables self-folding capacity upon exposure to humidity. By adjusting the copolymerization reaction time, we achieved a tunable bimodal molecular weight distribution, allowing us to customize the properties of the printed constructs. The incorporation of bioactive glass microparticles into the ink formulation improved resolution and preserved biocompatibility of DLP printed constructs. The versatility of DLP printing was demonstrated by creating complex structures. Tubular scaffolds with a programmed porosity pattern were built to serve as tissue scaffolds. The scaffolds exhibited around 90% cell viability and a clinically relevant biodegradability rate (≈50% mass loss after 4 weeks) which were ideal for tissue engineering applications. We showcased the dynamic capabilities of the printed constructs by creating grippers and film actuators. These structures demonstrated time dependent transformations in response to changes in environmental humidity. The capability of the material to act as a mechanical gripper was shown by lifting, transporting, and releasing a foam object ≈five times the film weight in response to controlled changes in humidity. The printed film functioned like a humidity actuator and folded upon proximity to skin. The programmable nature of the transformations, controlled by exposure time, light intensity, and the film thickness highlights the versatility of our ink to fabricate moisture-responsive smart materials. This offers exciting opportunities for developing adaptive materials and devices which function selectively based on the variations of the humidity of the environment. The developed synthetic ink establishes a foundation for future breakthroughs in tissue engineering and actuator design.

4. Experimental Section

Materials: Isopropanol (IPA) was used as a washing reagent. 1,6-hexamethylenediisocyanate (HDI) was used as a crosslinker, hydroxylethylacrylate (HEA) was used as a photocrosslinking agent, polyethylene-glycol (PEG) was used as a monomer, dibutyltindilaurate (DBTDL) was used as a catalyst, Comarin 6 was used as a florescent dye, Ponceau 4R food dye was used as a photo-absorber, lithium phenyl-2,4,6-trimethyl-benzoyl-phosphinate (LAP) and ruthenium:sodium-persulfate (Ru:SPS) were used as photoinitiators, and dimethylformamide (DMF) was used during synthesis as received from Sigma–Aldrich, Germany.

Synthesis of PEG-PU-DA Copolymers: Photocrosslinkable PEG-polyurethane (PU) copolymers have been synthesized through two step polymerization technique (Figure 2a). Before starting the reaction, predetermined amount of solid PEGs was added in a three neck flask and dissolved in DMF at 80 °C. Then, the solution was placed at 80 °C under continuous N_2 flow for 3 h to remove the traces of moisture. In the 1st step, pre-calculated amount of hexamethylene diisocyanate (HDI) was added in the PEG solution dropwise, maintaining the HDI:PEG molar ratio 2:1. After a predetermined reaction time, "Rt," hydroxyethyl acrylate (HEA) was added in the reaction mixture dropwise keeping the PEG:HEA molar ratio 2:1 to anchor acrylate groups to both ends of the linear chain. The solution was stirred overnight at 80 °C under inert atmosphere to achieve full conversion. To improve the conversion rate, 0.1 mL of 1 wt% catalyst (dibutyltin dilaurate, DBTDL) in toluene was added to the solution. Then, the aliquot was stored in a dark and sealed container. Some of the aliquot was dried under a reduced pressure at 60 °C for further analysis.

Preparation of PEG-PU-DA Inks: For printing, the ink, photo-initiator, and additives such as photo absorber, microparticles, and fluorescent additives were dissolved in a selective solvent such as Milli-Q water as described in following. The ink was prepared by mixing 500 μL of the synthesized PEG-PU-DA (having 15 wt% copolymer), with 500 μL Milli-Q water, stirring for 5 min till reaching a transparent homogeneous solution of low viscosity (<5 Pa.s), which hereinafter will be called "PEG-PU-DA" ink. The ink was mixed with a photo-initiator (PI). One of the following photoinitiators (PIs) was selected for each of the two 3D-printer setups used in this research: either LAP was used for printing the ink with a custom-built DLP printer that allowed printing at a very high intensity light (700 mW cm⁻² at the peak wavelength 380 nm) or Ru:SPS for preparing the ink with the 3D printer that allowed printing at a low intensity light (2 mW cm⁻² at the peak wavelength 400 nm). LAP stock solution was prepared by dissolving 10 mg LAP in 1 mL Milli-Q water followed by sonication for 20 min. For Ru:SPS, the standard protocol from AdvancedBiomatrix was utilized.[57] Briefly, 30 μL of the Ru stock solution was added to 1 mL of the prepared solution of PEG-PU-DA and Milli-Q water, stirred for 5 min; then, the same amount of SPS stock solution was added to the solution and stirred for 5 min; the ink then stored in cold and dark conditions for printing. Coumarin 6 (Sigma–Aldrich, St. Louis, MO) was used for fluorescent imaging and the results were converted to the red channel by ImageJ for better visibility. Coumarin 6 stock solution was prepared at a concentration of 20 mM in reagent ethyl alcohol (Sigma–Aldrich, St. Louis, MO). 30 μL of the stock solution was added to the mixture and stirred for 5 min before printing. To prepare the ink including, for example, 13% additives such as glass particles (or dye particles), 13 mg of the additive particles was added per 100 mg of the copolymer. 1 mL of the synthesized ink was equivalent to ≈150 mg of copolymer after being dried under vacuum (10 mbar, 60 °C) overnight.

GPC: Gel permeation chromatography (GPC) measurement was performed on an instrument having a SDV linear XL gel column (particle size = 5 μm) with separation range from 100 to 3 000 000 Da (PSS, Mainz, Germany) together with a refractive index detector (1200 Series, Agilent Technologies). $CHCl_3$ (HPLC grade) was used as solvent (for dissolving

polymer and as eluting solvent) with a flow rate of 0.5 mL min^{-1} at room temperature. As internal standard, toluene (HPLC grade) was used. The calibration was done with narrowly distributed polystyrene (PS) homopolymers (PSS calibration kit). An injection volume of 20 µL was used for the measurements. The sample was dissolved in CHCl$_3$ and filtered through a 0.22 µm PTFE filter before analysis. M_n, M_w, and PDI were calculated from the raw data according to the established method.

Rheology: Rheological studies were performed to determine viscosity (mPa.s) and shear stress (Pa) at a particular shear rate (s^{-1}). Studies were conducted using an Anton Paar rheometer with 50 mm parallel plate geometry, humidity control, and temperature control modules. A gap of 500 µm was used and the viscosity for each sample was evaluated using a steady state flow procedure. The shear rate was increased in a logarithmic progression for all inks. The device default algorithm was used to calculate the number of points per decade for recording the data at different temperatures.

Differential Scanning Calorimetry (DSC): DSC analysis of the dried ink samples before cross-linking, and crosslinked samples without glass and with glass microparticles were conducted using a DSC3 (Mettler Toledo, USA) under a nitrogen atmosphere. Crosslinked samples washed with ethanol before drying. Samples were dried in a vacuum oven at 10 mbar, 60 °C, overnight; then, were inserted to aluminum crucibles ($\approx$7 mg per crucible) and subjected to a three-step thermal cycle: first heated from 25 °C to 100 °C to remove prior history of the copolymer; then, cooled from 100 °C to -70 °C (2nd cycle), and finally heated again from -70 °C to 100 °C (3rd cycle). All thermal cycles were performed at a heating/cooling rate of 10 °C min^{-1}.

Tensile Tests: Tensile tests were performed under Anton–Paar as well as G2-TA DMA testing machine. Three replicates of rectangular samples (10 × 5 × 0.5 mm^3) were exposed to uniaxial tensile deformation at a constant rate of 1 mm min^{-1}, and best representatives were illustrated.

DLP 3D Printing at High Intensity Light: PEG-PU-DA ink was printed with our custom-built DLP 3D printer.[70] The DLP 3D printer was composed of a high precision linear stage (Newport Corp., Irvine, CA), a digital micro-mirror (DMD, Texas Instrument, Dallas. TX) with a lamp (Visitech; Wetzlar, Germany) of LED type working at high intensity (700 mW cm^{-2}, 380 nm wavelength) in the focal length. The printer had bi-axial movement in x–y direction controlled by a stepper motor synced by an Arduino UNO, and the z-axis was controlled by high precision linear stage. The entire printing sequence was controlled by an in-house made LabVIEW program. To print samples, predefined steps were followed. First, a computer-aided design (CAD) model was generated and sliced layer-by-layer. PEG-PU-DA was kept on a UV-Grade Petri dish (Soda Lime, Corning, NY), and consecutive printing layer-by-layer was performed by sequential action of z-axis stage and light exposure. The printer followed bottom-up approach for printing. To allow detaching each crosslinked layer, a thin layer of polydimethylsiloxane (PDMS) was applied to the glass substrate by applying spin coating (at a speed of $\approx$100 rpm). In the case of single layer printing, the thickness of the printed sample was limited by controlling the gap between the build platform (replaceable glass slide) and the substrate.

SLA 3D Printing at Low Intensity Light: Inks were mixed with 3:30 mM Ru:SPS photo initiator, different dye, and glass content; then, were exposed to low intensity light (2 mW cm^{-2} at 400 nm, Wanhao-Duplicator 7) for different exposure times according to the fractional factorial method. Optical microscopy images (top-view) and angle goniometer images (side-view) taken from the printed samples were used to measure the printed area and the cure depth, respectively (Figure 3a). Statistical analysis of the results was performed by MiniTab software. The optimal printing condition was defined to simultaneously maximize the cure depth and minimize the absolute value of the difference between the cure/printed area and the target photomask area (i.e., 1.2 mm^2). This target function was called "composite desirability" and illustrated in Figure S1f, Supporting Information.

Characterization of Folding: Rectangular samples (1.5 × 1 mm; length × width) of thickness 100 ± 20 µm were fabricated at different light exposure times (0.1, 0.2, 0.3, 0.4, and 0.5 s) upon a single step crosslinking (Figure 4a; Figure S2, Supporting Information). The thickness of the samples was controlled by limiting the cure depth by keeping the substrate and the build platform at a gap around 100 µm. The crosslinked samples

were dried in a vacuum oven (60 °C overnight) and immersed in water. The samples were imaged using florescent microscope (Nikon, Melville, NY) and analyzed using ImageJ software (NIH, Bethesda, MD). Folding behavior was analyzed at different exposure times (1, 2.5, 5, 7.5, and 10 s). The single-layer samples were then washed with IPA, dried overnight, and the folding experiments were conducted by submerging the dried samples in water. Folded samples were observed 10 min and 24 h after folding to check the folding dynamics and the stability of the programmed geometries. Succeeding the single step crosslinking, a two-step crosslinking approach was implemented to evaluate the folding behavior in multi-layer samples of different crosslinking at each layer. Different crosslinking density per layer was programmed by selecting different exposure time on each layer. The initial layer was printed at 0.4 s exposure time whereas the second layer was printed with a tenfold exposure time. All samples were printed on a non-coated glass slide. Printed samples were washed with IPA to remove the uncured resin and dried overnight; then, submerged in DI water for further observation of their folding dynamics.

Evaluation of Resolution: Subsequently after folding characterization, an optimal folding at a specific exposure time (i.e., 0.4 s) was obtained and was used to perform resolution analysis. An increasing pixelated bar pattern (Figure S3a, Supporting Information) was applied to study the resolution for the material in the authors' custom-built DLP printer. The pattern was arranged in a way that the width of each pattern exceeded the preceding pattern by one-pixel (theoretically for the DMD device; 1 pixel ≡ 7.5 microns); similar increment was set for space between patterns. For example, as shown in extended view (Figure S3–a, Supporting Information), the initial pattern was "x" pixel; then, for another pattern, a gap of "x" pixel was maintained; and, the next pattern was made of "x+1" pixels. The sample underwent one-step crosslinking and was washed with IPA. The samples were imaged using a fluorescent microscope and analyzed using ImageJ.

Studying the Effect of pH: The effect of pH on folding behavior of printed samples was analyzed by regulating the pH of submerging solutions. Rectangular samples (3.45 × 2.3 mm; length × width) with 12 equidistance square holes of 250 µm length were fabricated, making the profile symmetric in either direction (Figure S3-c-i-ii, Supporting Information). The pH of folding media was increased by adding sodium hydroxide in DI water, whereas the pH was decreased by adding acetic acid in DI water. For acidic solution, pH of solution was maintained at pH ≈ 2; for basic, it was set to pH ≈ 11; and for neutral, it was set to pH ≈ 7 using litmus papers. Same samples were printed, dried overnight, and submerged in the above solutions in a sequence: first into pH ≈ 2; then, pH ≈ 7; and later, pH ≈ 11 for 10 min. The samples were imaged and analyzed with ImageJ to figure out the influence of pH on the diameter of the formed tubes and their pore size.

Cell Culture Studies: MC3T3-E1 cells (with passage number below 7) was cultured on the printed scaffold. The printed scaffolds were fixed in the cell crowns (Scaffdex CellCrown inserts) and were washed with 70% ethanol and PBS before being sterilized with UV light under the bench for 30 min. To increase the cell adhesion on the scaffolds, they were coated with sterilized 20% collagen type IV solution in PBS for 1 min. Cell suspension of density 60 000 cells cm^{-2} was seeded on the scaffold and incubated for 1 h for an initial cell attachment. MC3T3-E1 cell line was cultured in the medium made of minimum essential medium (α-MEM) containing 10% fetal bovine serum (FBS) and 1% Pen/Strep. The culture medium was refreshed every 3 days.

Live/Dead Assay: Viability of MC3T3-E1 cells on the printed scaffolds was measured using Live–Dead assay at the time points: 1, 4, and 7 days after the culture. A cell staining solution containing 1 µL of Calcein AM (Invitrogen, Thermo Fisher) and 4 µL of Ethidium Homodimer-1 (EthD-1, Thermo Fisher) was prepared in 2 mL PBS, and the samples were covered with staining solution and incubated at room temperature for 20 min. Imaging of the samples was done using fluorescence microscopy (Nikon Ti2, Japan). The cell viability was analyzed by counting the number of live and dead cells in four different images using ImageJ, dividing the number of live cells to accumulative number of live and dead cells per image and drawing the average viability values and the standard deviations.

ADVANCED
SCIENCE NEWS

www.advancedsciencenews.com

NANO · MICRO

small

www.small-journal.com

Cell Metabolic Activity: The proliferation rate of MC3T3-E1 cells cultured on the printed scaffolds was measured using alamarBlue assay at the time points of 4 and 7 days after culture. 10% of alamarBlue solution was added to the scaffolds with 500 µL of MC3T3-E1 cell culture medium. The samples were incubated at 37 °C for ≈4 h. In order to avoid gradient formation, samples were gently rocked back and forth each 30 min. After incubation, the solution was collected from each sample and was kept on ice in the dark condition to stop the reaction. 100 µL of the aliquots was transferred to a 96-well plate to measure the fluorescence using a plate reader (BertholdTech TriStar2S, Germany) at an excitation wavelength of 535 nm and an emission wavelength of 590 nm. 10% alamarBlue in media without the cells and completely reduced alamarBlue were used as negative and positive control, respectively.

Degradation Tests: To study the degradation of the PEG-based material, the samples were immersed in DPBS solution at 37 °C and monitored at 1, 2, 3, and 4-week intervals. The DPBS solution was changed every 2 days and remained at a steady pH of 7 throughout the process. Degradation was carried out on 6-well plates, with each sample consisting of 5 × 10 mm dimension. To ensure accuracy, three replicates were performed for each sample. Following immersion, the samples were washed with Mili-Q water and freeze-dried before being measured. Mass loss was calculated using the following equation: Mass loss (%) = ([Initial Mass – Final Mass after time interval]/Initial Mass) × 100%. The degradation process was carried out in a stationary incubator.

Supporting Information

Supporting Information is available from the Wiley Online Library or from the author.

Conflict of Interest

The authors declare no conflict of interest.

Author Contributions

H.G.H performed the chemical synthesis, created the structures by light-assisted 3D printing, and prepared the supplemental videos/materials. A.Bi was a main contributor in the synthesis and polymer characterization. H.G.H and A.Bi equally contributed to the initial design of this study. A.Bh. and A.Y. equally contributed to carrying out the characterization experiments on produced films (self-folding and biocompatibility tests, respectively). A.L. contributed to DSC and swelling tests. H.G.H wrote the draft, A.K.M. and L.I. revised the manuscript. W.-H.Z., A.K.M., and L.I provided the facilities. All authors contributed to the revision of the paper.

Data Availability Statement

The data that support the findings of this study are available in the supplementary material of this article.

[1] D. Ahn, L. M. Stevens, K. Zhou, Z. A. Page, *ACS Cent. Sci.* **2020**, *6*, 1555.

[2] H. Goodarzi Hosseinabadi, D. Nieto, A. Yousefinejad, H. Fattel, L. Ionov, A. K. Miri, *Appl. Mater. Today* **2023**, *30*, 101721.

[3] K. Sertoglu, Desktop Metal unveils new expandable foam 3D printing material, FreeFoam –3D Printing Industry, https://3dprintingindustry.com/news/desktop-metal-unveils-new-expandable-foam-3d-printing-material-freefoam-21126, date accessed: 2022.07.06.

[4] W. Hua, W. Shi, K. Mitchell, L. Raymond, R. Coulter, D. Zhao, Y. Jin, *Chin. J. Mech. Eng. Addit. Manuf. Front.* **2022**, *1*, 100020.

[5] J. Young, Adidas-smart-factory-3D-printing, https://3dprint.com/162252/adidas-smart-factory-3d-printing, date accessed: 2023.09.1.

[6] E. Obasare, E. Melendres, D. L. Morris, S. K. Mainigi, G. S. Pressman, *Int. J. Cardiovasc. Imaging* **2016**, *32*, 1495.

[7] B. Zhang, R. Cristescu, D. B. Chrisey, R. J. Narayan, *Int. J. Bioprint.* **2020**, *6*, 211.

[8] S. I. Pop, M. Dudescu, S. G. Mihali, M. Pacurar, D. C. Bratu, *Polymers* **2022**, *14*, 2107.

[9] H. Goodarzi Hosseinabadi, E. Dogan, A. K. Miri, L. Ionov, *ACS Biomater. Sci. Eng.* **2022**, *8*, 1381.

[10] A. K. Miri, D. Nieto, L. Iglesias, H. Goodarzi Hosseinabadi, S. Maharjan, G. U. Ruiz-Esparza, P. Khoshakhlagh, A. Manbachi, M. R. Dokmeci, S. Chen, S. R. Shin, Y. S. Zhang, A. Khademhosseini, *Adv. Mater.* **2018**, *30*, 1800242.

[11] Y. Lu, G. Mapili, G. Suhali, S. Chen, K. Roy, *J. Biomed. Mater. Res., Part A* **2006**, *77*, 396.

[12] Q. Yuecheng, P. Wenjian, *3D Printing Photosensitive Resin for Precision Casting of Ornaments and Dentistry* **2017**, https://patents.google.com/patent/CN107603201B/en.

[13] J. L. Saorin, M. D. Diaz-Alemán, J. De La Torre-Cantero, C. Meier, I. Pérez Conesa, *Appl. Sci.* **2021**, *11*, 3197.

[14] X. Kuang, J. Wu, K. Chen, Z. Zhao, Z. Ding, F. Hu, D. Fang, H. J. Qi, *Sci. Adv.* **2019**, *5*, eaav5790.

[15] E. Dogan, A. Bhusal, B. Cecen, A. K. Miri, *Appl. Mater. Today* **2020**, *20*, 100752.

[16] H. Goodarzi Hosseinabadi, R. Bagheri, L. Avila Gray, V. Altstädt, K. Drechsler, *Polym. Test.* **2017**, *63*, 163.

[17] A. Cortés, A. Cosola, M. Sangermano, M. Campo, S. González Prolongo, C. F. Pirri, A. Jiménez-Suárez, A. Chiappone, *Adv. Funct. Mater.* **2021**, *31*, 2106774.

[18] M. Gastaldi, F. Cardano, M. Zanetti, G. Viscardi, C. Barolo, S. Bordiga, S. Magdassi, A. Fin, I. Roppolo, *ACS Mater. Lett.* **2021**, *3*, 1.

ADVANCED
SCIENCE NEWS
www.advancedsciencenews.com

NANO · MICRO
small
www.small-journal.com

[19] I. Apsite, S. Salehi, L. Ionov, *Chem. Rev.* **2022**, *122*, 1349.

[20] J. A. H. P. Sol, L. G. Smits, A. P. H. J. Schenning, M. G. Debije, *Adv. Funct. Mater.* **2022**, *32*, 2201766.

[21] W. Zhu, J. Li, Y. J. Leong, I. Rozen, X. Qu, R. Dong, Z. Wu, W. Gao, P. H. Chung, J. Wang, S. Chen, *Adv. Mater.* **2015**, *27*, 4411.

[22] V. Vitola, I. Bite, I. Apsite, A. Zolotarjovs, A. Biswas, *J. Polym. Res.* **2021**, *28*, 13.

[23] Y. Wang, H. Cui, Y. Wang, C. Xu, T. J. Esworthy, S. Y. Hann, M. Boehm, Y.-L. Shen, D. Mei, L. G. Zhang, *ACS Appl. Mater. Interfaces* **2021**, *13*, 12746.

[24] A. Kirillova, R. Maxson, G. Stoychev, C. T. Gomillion, L. Ionov, *Adv. Mater.* **2017**, *29*, 1703443.

[25] I. Apsite, A. Biswas, Y. Li, L. Ionov, *Adv. Funct. Mater.* **2020**, *30*, 1908028.

[26] S. You, J. Guan, J. Alido, H. H. Hwang, R. Yu, L. Kwe, H. Su, S. Chen, *J. Manuf. Sci. Eng.* **2020**, *142*, 081002.

[27] I. Apsite, G. Constante, M. Dulle, L. Vogt, A. Caspari, A. R. Boccaccini, A. Synytska, S. Salehi, L. Ionov, *Biofabrication* **2020**, *12*, 035027.

[28] I. Apsite, *Ph.D. Thesis*, Universität Bayreuth, **2020**.

[29] S. Miao, H. Cui, M. Nowicki, L. Xia, X. Zhou, S. Lee, W. Zhu, K. Sarkar, Z. Zhang, L. G. Zhang, *Adv. Biosyst.* **2018**, 1800101, 10.1002/adbi. 201800101.

[30] Z. Zhao, H. J. Qi, D. Fang, *Soft Matter* **2019**, *15*, 1005.

[31] Z. Zhao, X. Kuang, C. Yuan, H. J. Qi, D. Fang, *ACS Appl. Mater. Interfaces* **2018**, *10*, 19932.

[32] L. Yue, S. Macrae Montgomery, X. Sun, L. Yu, Y. Song, T. Nomura, M. Tanaka, H. Jerry Qi, *Nat. Commun.* **2023**, *14*, 1251.

[33] Y. Chen, J. Zhang, X. Liu, S. Wang, J. Tao, Y. Huang, W. Wu, Y. Li, K. Zhou, X. Wei, S. Chen, X. Li, X. Xu, L. Cardon, Z. Qian, M. Gou, *Sci. Adv.* **2020**, *6*, eaba7406.

[34] A. K. Miri, H. Goodarzi Hosseinabadi, B. Cecen, S. Hassan, Y. S. Zhang, *Acta Biomater.* **2018**, *140*, 170.

[35] Y. Shen, H. Tang, X. Huang, R. Hang, X. Zhang, Y. Wang, X. Yao, *Carbohydr. Polym.* **2020**, *235*, 115970.

[36] G. Melilli, I. Carmagnola, C. Tonda-Turo, F. Pirri, G. Ciardelli, M. Sangermano, M. Hakkarainen, A. Chiappone, *Polymers* **2020**, *12*, 1655.

[37] A. Thomas, I. Orellano, T. Lam, B. Noichl, M.-A. Geiger, A.-K. Amler, A.-E. Kreuder, C. Palmer, G. Duda, R. Lauster, L. Kloke, *Acta Biomater.* **2020**, *117*, 121.

[38] T. Lam, T. Dehne, J. P. Krüger, S. Hondke, M. Endres, A. Thomas, R. Lauster, M. Sittinger, L. Kloke, *J. Biomed. Mater. Res., Part B* **2019**, *107*, 2649.

[39] S. H. Kim, Y. K. Yeon, J. M. Lee, J. R. Chao, Y. J. Lee, Y. B. Seo, M. T. Sultan, O. J. Lee, J. S. Lee, S. Il Yoon, I. S. Hong, G. Khang, S. J. Lee, J. J. Yoo, C. H. Park, *Nat. Commun.* **2018**, *9*, 1620.

[40] G. C. Berry, *J. Rheol.* **1996**, *40*, 1129.

[41] E. Askari, M. Akbari, in *Addit. Manuf. Biopolym*, Elsevier, **2023**, pp. 265, https://www.sciencedirect.com/science/article/abs/pii/B9780323951517000003X.

[42] Q. Ramadan, M. Zourob, *Front. Med. Technol.* **2021**, *2*, 607648.

[43] D. M. Kirchmajer, R. Gorkin, M. In Het Panhuis, *J. Mater. Chem. B* **2015**, *3*, 4105.

[44] M. Regehly, Y. Garmshausen, M. Reuter, N. F. König, E. Israel, D. P. Kelly, C.-Y. Chou, K. Koch, B. Asfari, S. Hecht, *Nature* **2020**, *588*, 620.

[45] D. Raviv, W. Zhao, C. Mcknelly, A. Papadopoulou, A. Kadambi, B. Shi, S. Hirsch, D. Dikovsky, M. Zyracki, C. Olguin, R. Raskar, S. Tibbits, *Sci. Rep.* **2014**, *4*, 6.

[46] S. Tibbits, *Archit. Des.* **2014**, *84*, 116.

[47] Y.-Q. Liu, J.-N. Ma, Y. Liu, D.-D. Han, H.-B. Jiang, J.-W. Mao, C.-H. Han, Z.-Z. Jiao, Y.-L. Zhang, *Opt. Mater. Express* **2017**, *7*, 2617.

[48] M. Zhang, A. Arunachalam, H. Perrin, S. Polat, J. Groenewold, E. Mendes, H. B. Eral, H. B. Eral, *ACS Appl. Polym. Mater.* **2023**, *5*, 4780.

[49] Y. He, J. Guo, X. Yang, B. Guo, H. Shen, *RSC Adv.* **2021**, *11*, 37744.

[50] C. A. Spiegel, M. Hackner, V. P. Bothe, J. P. Spatz, E. Blasco, *Adv. Funct. Mater.* **2022**, *32*, 2110580.

[51] Y. Jiang, Q. Y. Leng, Y. Yan, E. L. L. Ng, H. L. Chee, F. Wang, S. Y. Chan, X. J. Loh, J. Wang, B. Q. Y. Chan, *ACS Appl. Polym. Mater.* **2022**, *4*, 8574.

[52] S. Armon, E. Efrati, R. Kupferman, E. Sharon, *Science* **2011**, *333*, 1726.

[53] Y. Hu, Q. Shang, C. Bo, P. Jia, G. Feng, F. Zhang, C. Liu, Y. Zhou, *ACS Omega* **2019**, *4*, 12505.

[54] A. Biswas, V. K. Aswal, B. Ray, P. Maiti, *J. Phys. Chem. C* **2018**, *122*, 11167.

[55] R. J. Mondschein, A. Kanitkar, C. B. Williams, S. S. Verbridge, T. E. Long, *Biomaterials* **2017**, *140*, 170.

[56] S. Schüller-Ravoo, S. M. Teixeira, J. Feijen, D. W. Grijpma, A. A. Poot, *Macromol. Biosci.* **2013**, *13*, 1711.

[57] K. S. Lim, R. Levato, P. F. Costa, M. D. Castilho, C. R. Alcala-Orozco, K. M. A. van Dorenmalen, F. P. W. Melchels, D. Gawlitta, G. J. Hooper, J. Malda, T. B. F. Woodfield, *Biofabrication* **2018**, *10*, 034101.

[58] W. Li, M. Wang, L. S. Mille, J. A. Robledo Lara, V. Huerta, T. Uribe Velázquez, F. Cheng, H. Li, J. Gong, T. Ching, C. A. Murphy, A. Lesha, S. Hassan, T. B. F. Woodfield, K. S. Lim, Y. S. Zhang, *Adv. Mater.* **2021**, *33*, 2102153.

[59] M. Cannio, D. Bellucci, J. A. Roether, D. N. Boccaccini, V. Cannillo, *Materials* **2021**, *14*, 5440.

[60] Getting Started with Minitab Statistical Software, Minitab.Company, **2022**.

[61] C. F. Bellani, K. Yue, F. Flaig, A. Hébraud, P. Ray, N. Annabi, H. S. Selistre De Araújo, M. C. Branciforti, A. M. Minarelli Gaspar, S. R. Shin, A. Khademhosseini, G. Schlatter, *Biofabrication* **2021**, *13*, 035020.

[62] J. Zhang, Y. Sakisaka, H. Ishihata, K. Maruyama, E. Nemoto, S. Chiba, M. Nagamine, H. Hasegawa, S. Yamada, *Materials* **2020**, *13*, 5288.

[63] S. M. Panda, H. G. Hosseinabadi, H. Fattel, U. Tripathy, A. K. Miri, *ACS Appl. Opt. Mater.* **2023**, https://doi.org/10.1021/acsaom. 3c00165.

[64] L. Ouyang, Y. Dan, Z. Shao, S. Yang, C. Yang, G. Liu, D. Duan, *Exp. Ther. Med.* **2019**, *18*, 2933.

[65] J. Wei, S. Jia, J. Guan, C. Ma, Z. Shao, *ACS Appl. Mater. Interfaces* **2021**, *13*, 54417.

[66] An early bloom of evolution – Florida Museum of Natural History, https://www.floridamuseum.ufl.edu/science/an-early-bloom-of-evolution, date accessed: 2023.03.15.

[67] M. F. Simon, R. Grether, L. P. De Queiroz, T. E. Särkinen, V. F. Dutra, C. E. Hughes, *Am. J. Bot.* **2011**, *98*, 1201.

[68] L. Yao, J. Ou, G. Wang, C. Y. Cheng, W. Wang, H. Steiner, H. Ishii, *3D Print. Addit. Manuf.* **2015**, *2*, 169.

[69] A. Sydney Gladman, E. A. Matsumoto, R. G. Nuzzo, L. Mahadevan, J. A. Lewis, *Nat. Mater.* **2016**, *15*, 413.

[70] A. Bhusal, E. Dogan, H.-A. Nguyen, O. Labutina, D. Nieto, A. Khademhosseini, A. K. Miri, *Biofabrication* **2022**, *14*, 014103.

2306387 (13 of 13)